IEEE Access
Multidisciplinary | Rapid Review | Open Access Journal

Received 31 May 2023, accepted 20 June 2023, date of publication 23 June 2023, date of current version 28 June 2023.

Digital Object Identifier 10.1109/ACCESS.2023.3288902

RESEARCH ARTICLE

Fractional Order Nonsingular Terminal Sliding Mode Cooperative Fault-Tolerant Control for High-Speed Trains With Actuator Faults Based on Grey Wolf Optimization

BINCHUAN LIANG[1] **AND TONG ZHANG**[2]
[1]College of Automation and Electrical Engineering, Dalian Jiaotong University, Dalian 116028, China
[2]College of Locomotive and Rolling Stock Engineering, Dalian Jiaotong University, Dalian 116028, China
Corresponding author: Tong Zhang (zhang_tong66@126.com)

ABSTRACT This paper mainly studies the cooperative precise control of multiple high-speed trains under external random interference. The safety distance potential energy function is introduced to constrain the safety distance between trains, and the output control quantity is adjusted rapidly in real-time. An effective fractional nonsingular terminal sliding surface is designed to ensure that the system can quickly converge to the equilibrium point while reducing buffeting. The double-loop recurrent neural network with better approximation ability is used to approximate the external interference during high-speed train operation and update the parameters in real-time. Aiming at the possible actuator failure during train operation, a high-robustness fractional nonsingular terminal sliding mode controller is designed, and its stability and convergence are proved by using Lyapunov stability theory. Based on the idea of inertia weight and the nonlinear position update strategy of convergence factor, an improved grey wolf optimization algorithm is proposed to obtain the optimal parameters of the control system. The simulation results show that the method designed in this paper can accurately track the ideal speed and displacement, and has better control accuracy, ideal fault-tolerance, robustness and stability compared with other control methods.

INDEX TERMS High-speed train, random interference, fractional terminal sliding mode, double loop recurrent neural network, grey wolf optimization.

I. INTRODUCTION

The transportation system plays an important role in promoting the development of China's entire industrialization, and its operation and construction have an important impact on China's new industry to a certain extent. With the rapid development of high-speed train technology, advanced high-speed train technology plays a vital role in promoting the development of China's railway transportation [1]. The control technology of key systems of high-speed trains is not only related to the smooth and safe operation of high-speed trains but also the concentrated embodiment of the development of cutting-edge high-speed railway technology [2]. The traction and braking system of high-speed trains has a complex structure. Its actuator often works under high loads and frequently switches, which is prone to failure, thus seriously affecting the safe operation of trains [3]. The adoption of more advanced control methods is a solution to ensure the safe and reliable operation of high-speed trains. Due to the huge nonlinearity and uncertainty of high-speed train operation, it is necessary to design an appropriate robust controller.

Sliding mode control is widely used in the control of various nonlinear objects and traction and braking systems of high-speed trains because of its insensitivity to model errors, parameter changes, and external disturbances [4]. As an improved algorithm of sliding mode control, nonsingular terminal sliding mode control has the advantages of converging to the sliding mode equilibrium point in a finite

The associate editor coordinating the review of this manuscript and approving it for publication was Emanuele Crisostomi.

time and generating small chattering, and will not produce singular phenomena of terminal sliding mode control in the process of variable convergence [5]. It has been proven to be a reliable sliding mode control algorithm. However, the traditional sliding mode control is usually integer-order control, and the control system will produce an obvious chattering phenomenon and slow convergence [6]. The introduction of fractional order makes the controlled object of the control system be represented by fractional order. The integration of fractional order control and sliding mode control makes the controlled systems have higher control accuracy and robustness [7]. This paper applies the fractional nonsingular terminal sliding mode fault-tolerant control technology to the control of the traction braking system and other key parts of high-speed trains under the condition of actuator-failure, which is of great significance to improve the stability, safety and system control precision of high-speed trains.

Fractional order Sliding mode control has a good control effect on nonlinear systems with uncertainties and external disturbances [8]. Sabatier et al. [9] proposed a fractional-order robust controller, which can use its characteristics to compensate for the change of the parameters of the controlled object so that the dynamic performance of the system is no longer affected by the uncertainty of the system parameters. Kaczorek et al. [10] derived the solutions of a group of matrix linear differential equations with different fractional orders. Pashaei et al. [6] designed sliding mode controller for the nonlinear system based on fractional order reaching law, analyzed the effect of fractional order on the performance of the controller and the accessibility of sliding mode surface under different initial conditions, and verified the effectiveness and superiority of the controller on the DC motor system. Razmi et al. [7] proposed a new position and attitude tracking control method for four-rotor UAVs in the presence of parameter uncertainty and external interference. This method combined a neural network adaptive scheme with sliding mode control and retained the advantages of the two methods. SEONGIK [11] has studied a new fractional-order nonsingular terminal sliding mode control (FTSMC), in which all parameters of the controller and observer were optimized using the improved grey wolf optimization (MGWO) technology, and this algorithm had a good control effect on the control of the manipulator. Zhang et al. [12] designed an adaptive fractional nonsingular fast terminal sliding mode control scheme using a disturbance observer to achieve trajectory tracking control of uncertain robots.

During high-speed train operation, some minor actuator faults will reduce train operation performance and increase operation instability [13]. With the increasing complexity of the high-speed train control system, the possibility of actuator failure in the actual control process is increasing [14], which makes the controller lose efficiency or completely damaged during operation [15], and brings huge hidden dangers to the safe operation of the train. Therefore, in recent years, the research on fault-tolerant control methods for automatic train operation has received widespread attention [16]. Mao et al. [17] proposed an adaptive fault-tolerant sliding mode control scheme for high-speed trains, established a dynamic model of actuator uncertainty based on the uncertainty of the input distribution matrix, and designed an adaptive sliding mode fault-tolerant controller to ensure that the tracking error is convergent within a certain time. Guo et al. [18] designed an adaptive fault-tolerant pseudo-PID sliding mode control scheme to reduce the impact of actuator failure and nonlinear actuator saturation integral quadratic constraints on high-speed trains. Liu et al. [19] established a model to represent unknown time-varying parameters in mathematical form and proposed an adaptive backstepping fault-tolerant controller to realize position tracking aiming at the problem of nonlinear time-varying parameters and actuator faults of high-speed trains. Dong et al. [20] considered the basic resistance, additional resistance, and workshop force of the train, established the multi-particle model of the train, and proposed a multi-dimensional sliding surface with time-varying parameters based on adaptive estimation technology for the unknown disturbance of the system. Song et al. [21] considered the force between vehicles and the dynamic model of actuator failure, and the fault-tolerant control algorithm proposed only requires the input and output response signal of traction/braking force.

The above literature considered the design of a fault-tolerant controller for a single high-speed train, but in reality, multiple high-speed trains usually operate on the same line. How to ensure the safe and coordinated operation of multiple high-speed trains in the event of actuator failure has not been fully considered. And there is not a sufficient discussion on the optimization of a large number of uncertain parameters in control systems. High-speed trains are influenced by the complex operating environment, resulting in differences in actual speeds between adjacent trains. So it is necessary to design a multi-train collaborative cruise controller to ensure that all trains ultimately reach the same speed and displacement while maintaining a safe distance to avoid collisions. Considering the huge amount of unknown parameters in the process of multi-train collaborative operation, it is necessary to design a high-precision and fast convergence parameter optimization algorithm.

The research background of the Grey Wolf Optimization(GWO) algorithm is an optimization algorithm based on the predation behavior of the grey wolf population. It was proposed by Mirjalili, a scholar at Griffith University in Australia, in 2014. It has been proven to be a relatively feasible optimization algorithm with good global search ability and fast convergence [22]. Wen et al. [23] improved the original GWO and skillfully used the penalty function method when dealing with constraint conditions, successfully transforming the research problem of non-stationary multi-stage allocation into an unconstrained optimization problem, solving the multi-stage allocation problem. Sihag et al. [24]

designed a new one-dimensional and full-dimensional hybrid selection strategy for the grey wolf population to balance exploration and development in the optimization process, using perturbation operators to maintain population diversity and improve the system's global search ability. Singh et al. [25] proposed a new hybrid algorithm GWO-PSO based on the combination of the Grey Wolf Optimization algorithm and Particle Swarm Optimization algorithm. The main idea of this hybrid algorithm was to further improve the search intensity of the algorithm based on improving the exploration ability of GWO and the mining ability of PSO. In the field of wireless sensor networks, Fouad et al. [26] proposed a method of node location based on the GWO algorithm. The algorithm established an objective function by finding nodes with a large number of adjacent nodes. Zhang et al. [27] used the GWO algorithm to solve the pathfinding problem of unmanned aerial vehicles (ACVs). The GWO algorithm tried three different dimensions of path planning problems, and found a safe path with the minimum fuel cost and avoided many threat areas. At the same time, the author also compared many other meta-heuristic algorithms, and the result was that the GWO algorithm can show its advantages more. Mosavi et al. [28] proposed a GWO algorithm for training multi-layer perceptive neural networks. Aljarah et al. [29] proposed a new GWO-inspired clustering analysis method based on location information and gave competitive results.

This paper considers the situation of actuator failure during the collaborative operation of multiple trains and designs a fractional order nonsingular terminal sliding mode collaborative fault-tolerant controller, The main innovation points of this paper:

(1) The safety distance potential energy function is introduced to constrain the safety distance of multiple trains, and the output control quantity is adjusted rapidly in real-time to ensure the safe distance between trains.

(2) The fractional nonsingular terminal sliding mode surface is designed to make the state variables have better global correlation, achieve more refinement and fast convergence of control, and reduce the chattering phenomenon of sliding mode control.

(3) The double-loop recurrent neural network is introduced to approximate the external interference during high-speed train operation, and the external interference is accurately estimated in real-time by updating the control rate.

(4) An improved grey wolf optimization algorithm is proposed to obtain the optimal global control parameters to ensure the optimal control of the system.

This paper designs a distributed collaborative fault-tolerant controller that enables high-speed trains to accurately track target displacement velocity and synchronize current state information. The other structure of this paper is as follows: In the second section, a dynamic model of cooperative control of multiple high-speed trains is established to simulate the random actuator failure that may occur during train operation, the actuator-failure factor is introduced, and the distance potential energy function is proposed to ensure the safe distance between trains. In the third section, a fractional-order nonsingular terminal sliding mode control method is designed. The double-loop recurrent neural network is introduced to approximate the external random nonlinear disturbance, the adaptive law is used to update the control parameters online, and the stability of the control system is analyzed. In the fourth section, based on the idea of nonlinear inertia weight and convergence factor, an improved grey wolf optimization algorithm is proposed to optimize the uncertain parameters of the control system. The fifth section is simulation analysis, and the sixth section is the conclusion.

II. SYSTEM DESCRIPTION

This section describes the dynamic model of cooperative control of multiple high-speed trains, introduces the actuator-failure factor, and constrains the conditions of cooperative control between trains based on the distance potential energy function.

A. MULTI-TRAIN DYNAMICS MODEL

For the convenience of description, each train is generally regarded as a rigid particle. The dynamic model of multi-train cooperative operation under ideal conditions is as follows:

$$\begin{cases} \dot{x_i}(t) = v_i(t) \\ \dot{v_i}(t) = \xi[u_i(t) - f_i(t)] \\ f_i(t) = f_{i0}(t) + f_{ir}(t) + f_{ic}(t) + f_{it}(t) \\ \xi = \dfrac{0.0098}{1+d} \end{cases} \tag{1}$$

where $x_i(t)$ is the displacement of the i_{th} high-speed train running on the same track, $v_i(t)$ is the speed of the i_{th} train, ξ is the acceleration coefficient, d is the train rotational mass coefficient (that is, the ratio of the train rotational mass to the total mass of the train), $u_i(t)$ is the unit control force of the ith high-speed train, $f_i(t)$ is the running resistance of the i_{th} high-speed train in the running process, $f_{i0}(t)$ is the unit general resistance of the i_{th} train, $f_{ir}(t)$, $f_{id}(t)$, $f_{it}(t)$ is the special additional resistance of the i_{th} high-speed train in the running process, $f_{ir}(t)$ is the unit ramp resistance and $f_{id}(t)$ is the unit curve resistance, $F_{it}(t)$ is the unit tunnel resistance, which can be described as:

$$\begin{cases} f_{i0}(t) = a_{i0} + a_{i1}(t)v_i(t) + a_{i2}(t)v_i(t)^2 \\ f_{ir}(t) = 1000\sin\theta_i(t) \approx 1000\tan\theta_i(t) \\ f_{ic}(t) = \dfrac{600}{R_i(t)} \\ f_{it}(t) = 0.000013L_i(t) \end{cases} \tag{2}$$

where a_{i0} is the rolling resistance coefficient, a_{i1} is the other mechanical resistance coefficient, which is proportional to the running speed of the i_{th} high-speed train, and a_{i2} is the external air resistance coefficient, which is proportional to the square of the running speed of the i_{th} high-speed train; $\theta_i(t)$ is the gradient angle of the track, $R_i(t)$ is the curve radius of the curve track, and $L_i(t)$ is the length of the tunnel.

B. FAULT MODEL OF TRAIN ACTUATOR

The actuator in the traction braking device of the train is often in a state of high-load operation. If the electrical components fail, the system will have actuator failure, which will cause the output of the traction system to deviate from the expected output [17]. In this paper, the failure and bias fault of the train actuator are considered. The fault model of the i_{th} train is expressed as:

$$\lambda_j(t) = \begin{cases} 1, & t < t_1 \\ \lambda_1(t), & t_1 \le t < t_2 \\ \lambda_2(t), & t_2 \le t < t_3 \\ \vdots & \\ \lambda_n(t), & t_n \le t < t_{n+1}. \end{cases} \tag{3}$$

where t_1 is the time of fault occurrence, $j = 1, 2, 3$. According to (3), when the actuator fails, the unit train control quantity will shift, affecting the safe operation of the train.

When actuator failure occurs, the dynamic model of the i_{th} high-speed train can be described as:

$$\begin{cases} \dot{x}_i(t) = v_i(t) \\ \dot{v}_i(t) = \xi[\lambda_i(t)u_i(t) - f_i(t)] \\ f_i(t) = f_{i0}(t) + f_{ir}(t) + f_{ic}(t) + f_{it}(t) \\ \xi = \dfrac{0.0098}{1+d} \end{cases} \tag{4}$$

C. CONSTRAINTS OF MULTI-TRAIN COOPERATIVE CONTROL

When multiple high-speed trains are running on the same line, real-time information such as train speed and position is collected through GSM-R and sent to the radio block center (RBC), which sends the information to the communication equipment of adjacent high-speed trains to activate the distance monitoring module, so that multiple trains can calculate the minimum safe distance $L_{\min}(t)$ and track the train in front under the moving block mode. Figure 1 is a schematic diagram of train coordinated operation.

To ensure the operation safety of high-speed trains on the same line, there must be a certain safety interval between trains, which is determined based on the maximum braking distance, redundant distance, length of the train itself, etc [30], as described below:

$$L_{\min}(t) = L_a(t) + L_b(t) + L_s(t) + L_t \tag{5}$$

where $L_a(t)$ is the additional safety distance, $L_b(t)$ is the maximum braking distance, $L_s(t)$ is the redundant distance, and L_t is the length of the high-speed train itself, as described below:

$$\begin{cases} L_a(t) = t_v v(t) \\ L_b(t) = \sum \dfrac{v_0(t) - v_t(t)}{2a} \\ L_s(t) = C + 0.5v(t) \end{cases} \tag{6}$$

where t_v is the travel time of the train after braking, $v_0(t)$ and $v_t(t)$ are the initial and final speed of the train within the braking sampling time, a is the average acceleration during the sampling process, and C is a constant parameter.

Then the constraint conditions of the designed control system can be described as follows:

$$X_{i-1}(t) - X_i(t) > L_{\min}(v(t)) \tag{7}$$

$X_{i-1}(t)$ and $X_i(t)$ represent the actual running distance of two adjacent trains.

The distance between adjacent high-speed trains should be kept within a safe range, which can be achieved by introducing artificial potential functions. The introduced potential energy function needs to meet the following requirements: when the distance is within the safe range, the potential energy is very small, but once the distance is close to the safe distance, the energy increases rapidly [31]. Define the following safety distance potential energy function:

$$U_{ij}\left(x_{ij}\right) = \frac{L_{\max}^2 - L_{\min}^2}{\left(x_{ij}^2 - L_{\min}^2\right)\left(L_{\max}^2 - x_{ij}^2\right)} \tag{8}$$

x_{ij} represents the safety distance between the i_{th} train and the j_{th} train, $L_{\min}$ represents the minimum safety distance, and $L_{\max}$ represents the maximum safety distance. Once the distance between trains approaches the maximum or minimum safe distance, it shall be restored to the safe range as soon as possible. The corresponding control component is represented as:

$$u_j = \rho \cdot \sum(-\nabla U_{ij}) \tag{9}$$

where ρ is a preset parameter. ∇U_{ij} is the value of gradient, the negative sign in front of which indicates a negative gradient direction.

III. COLLABORATIVE CONTROL SCHEME DESIGN

In this paper, a fractional-order nonsingular terminal sliding mode fault-tolerant control scheme based on the Grey Wolf Optimization algorithm is proposed to ensure the safe and stable operation of high-speed trains in the case of external random nonlinear interference and actuator failure. Figure 2 is the block diagram of the fractional-order nonsingular terminal sliding mode fault-tolerant control system. The overall control strategy is as follows:

As shown in Figure 2, the expected value $x_{d,i}(t)$, $v_{d,i}(t)$ are the inputs of the train ATO system. The errors $e_{x,i}(t)$, $e_{v,i}(t)$ can be calculated from the expected inputs $x_{d,i}(t)$, $v_{d,i}(t)$ and the actual outputs $x_i(t)$, $v_i(t)$. The actual outputs $x_i(t)$, $v_i(t)$ of the train are also the inputs of the DLRNN, which is used to calculate the external disturbance estimation value $\hat{f}_{d,i}(v(t))$, then $S_i(t)$ can be got through the fractional nonsingular terminal sliding mode surface. After that, the equivalent control term $u_{eqi}(t)$ is calculated from the errors $e_{x,i}(t)$, $e_{v,i}(t)$, the estimated value of external disturbance $\hat{f}_{d,i}(v(t))$ and the sliding mode surface function $S_i(t)$. At the same time, the approximation error compensation term $\hat{\varepsilon}_i(t)$ is calculated from $S_i(t)$.The control rate $\alpha_i(t)$ can be obtained by combining the equivalent control term $u_{eqi}(t)$

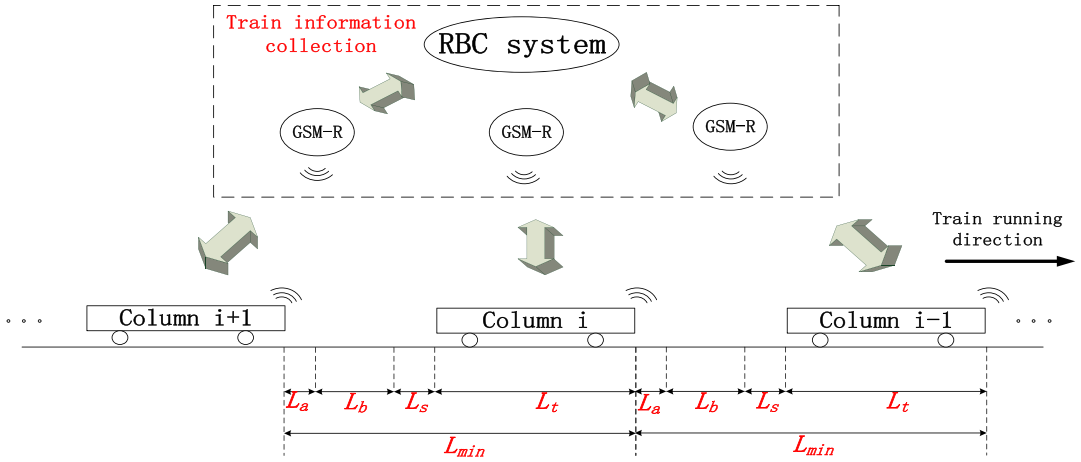

FIGURE 1. Schematic diagram of multi-train cooperative operation.

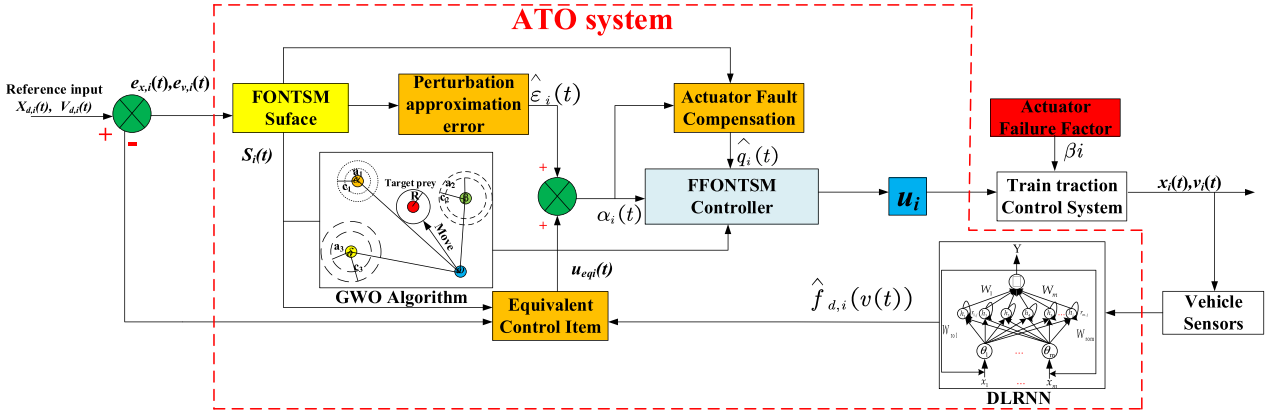

FIGURE 2. Overall structure block diagram of control system.

and the approximation error compensation term $\hat{\varepsilon}_i(t)$. $\alpha_i(t)$ and $S_i(t)$ are calculated to obtain the fault compensation term $\hat{q}_i(t)$. After obtaining the control rate and fault compensation information, the fractional order nonsingular terminal sliding mode controller outputs the control quantity to the train traction system. At the same time, the vehicle sensors obtain the actual outputs $x_i(t)$, $v_i(t)$ of each carriage at the sampling time, and feed them back to the ATO system.The grey wolf optimization algorithm is used to optimize the control parameters. The virtual control quantity is calculated by the controller in combination with the current reference inputs $x_{d,i}(t)$, $v_{d,i}(t)$. The above steps are repeated, so that effective fault-tolerant control of the train can be achieved.

A. DESIGN OF THE FRACTIONAL-ORDER NONSINGULAR TERMINAL SCREEN CONTROLLER

In order to improve the accuracy and convergence speed of the controller, this paper applies fractional differential to nonsingular terminal sliding mode control, which can effectively suppress the chattering phenomenon of sliding mode control, and obtains higher accuracy and faster convergence speed of the control system.

Let $x_d(k) \in \mathrm{R}^n$ and $v_d(k) \in \mathrm{R}^n$ be the expected position and expected speed of the train respectively. The position tracking error and speed tracking error of the ith train are defined as:

$$\begin{cases} e_{x_i}(k) = x_{d_i}(k) - x_i(k) \\ e_{v_i}(k) = v_{d_i}(k) - v_i(k). \end{cases} \tag{10}$$

Combining the common nonsingular terminal sliding mode control and fractional calculus theory [5], a fractional nonsingular terminal sliding mode surface is designed, which is defined as follows:

$$S_i(t) = e_{x_i}(t) + \beta_i^{-1} e_{v_i}(t)^{\frac{p_i}{q_i}} + D^{\alpha} e_{x_i}(t) \tag{11}$$

where, $\beta_i > 0$, p_i and $q_i (p_i > q_i)$ are positive odd numbers, and $1 < p_i/q_i < 2$, n>1, D^{α} is a fractional calculus operator, whose definition as (12), and $-1 < \alpha < 1$:

$${}_bD_t^{\alpha} = \begin{cases} \dfrac{\mathrm{d}^{\alpha}}{\mathrm{d}t^{\alpha}} & \mathrm{Re}(\alpha) > 0 \\ 1 & \mathrm{Re}(\alpha) = 0 \\ \displaystyle\int_0^t (d\tau)^{-\alpha} & \mathrm{Re}(\alpha) < 0 \end{cases} \tag{12}$$

where b and t are the upper and lower limits of differential or integral, α is an arbitrary real number. When the real part is greater than zero, the operator is a fractional order differential operator. When the real part is less than zero, the operator is a fractional order integral operator. Derivation of sliding surface:

$$\dot{S}_i = e_{v_i}(t) + \beta_i^{-1}\frac{p_i}{q_i}e_{v_i}^{\frac{p_i}{q_i}-1}\dot{e_{v_i}} + D^{\alpha}e_{v_i} \tag{13}$$

Substitute (1) into (13). There are:

$$\dot{S}_i = e_{v_i}(t) + \beta_i^{-1}\frac{p_i}{q_i}e_{v_i}^{\frac{p_i}{q_i}-1}\left\{\dot{v_{d_i}}(t) - \xi[u_i(t) - f_i(t)]\right\} + D^{\alpha}e_{v_i} \tag{14}$$

The general constant velocity approach law is selected as:

$$\dot{S}_i = -\frac{p_i}{q_i}e_{v_i}^{\frac{p_i}{q_i}-1}\sigma sgn(s), \sigma > 0 \tag{15}$$

Substitute (15) into (14) to obtain:

$$\begin{aligned}
&e_{v_i}(t) + \beta_i^{-1}\frac{p_i}{q_i}e_{v_i}^{\frac{p_i}{q_i}-1}(t)\left\{\dot{v}_{d_i}(t) - \xi[\lambda_j u_i(t) - f_i(t)]\right\} + D^{\alpha}e_{v_i}(t)\\
&= -\frac{p_i}{q_i}e_{v_i}^{\frac{p_i}{q_i}-1}\sigma sgn(s)\\
&\Rightarrow \beta_i^{-1}\frac{p_i}{q_i}e_{v_i}^{\frac{p_i}{q_i}-1}\left\{\dot{v_{d_i}}(t) - \xi[\lambda_j u_i(t) - f_i(t)]\right\}\\
&= -(\frac{p_i}{q_i}e_{v_i}^{\frac{p_i}{q_i}-1}\sigma sgn(s) + e_{v_i}(t) + D^{\alpha}e_{v_i})\\
&\Rightarrow \left\{\dot{v_{d_i}}(t) - \xi[\lambda_j u_i(t) - f_i(t)]\right\}\\
&= -\beta_i\left[\sigma sgn(s) + \frac{q_i}{p_i}e_{v_i}^{2-\frac{p_i}{q_i}}(t) + \frac{q_i}{p_i}D^{\alpha}e_{v_i}^{2-\frac{p_i}{q_i}}(t)\right]\\
&\Rightarrow u_i(t) = \frac{\beta_i}{\lambda_j\xi}\left[\sigma sgn(s) + \frac{q_i}{p_i}e_{v_i}^{2-\frac{p_i}{q_i}}(t) + \frac{q_i}{p_i}D^{\alpha}e_{v_i}^{2-\frac{p_i}{q_i}}(t)\right]\\
&+ \frac{\dot{v_{d_i}}(t)}{\lambda_j\xi} + \frac{1}{\lambda_j}f_i(t)
\end{aligned} \tag{16}$$

Control law:

$$\begin{aligned}
u_i(t) = &\frac{\beta_i}{\lambda_j\xi}\left[\sigma sgn(s) + \frac{q_i}{p_i}e_{v_i}^{2-\frac{p_i}{q_i}}(t) + \frac{q_i}{p_i}D^{\alpha}e_{v_i}^{2-\frac{p_i}{q_i}}(t)\right]\\
&+ \frac{\dot{v_{d_i}}(t)}{\lambda_j\xi} + \frac{1}{\lambda_j}f_i(t)
\end{aligned} \tag{17}$$

The stability is proved as follows:

The stability of the proposed fractional order nonsingular terminal sliding mode control (FONTSMC) method is discussed, and Lyapunov function $V = \frac{1}{2}S^2$ is selected.

Then when (18) is established, the system is progressively stable.

$$\dot{V} = S_i\dot{S}_i \le 0 \tag{18}$$

That is:

$$\begin{aligned}
\dot{V} &= S_i \bullet \left[e_{v_i}(t) + \beta_i^{-1}\frac{p_i}{q_i}e_{v_i}^{\frac{p_i}{q_i}-1}\dot{e_{v_i}} + D^{\alpha}e_{v_i}\right]\\
&= S_i \bullet \left[e_{v_i}(t) + \beta_i^{-1}\frac{p}{q}e_{v_i}^{\frac{p}{q}-1} \bullet \xi[u_i(t) - f_i(t)] + D^{\alpha}e_{v_i}\right]
\end{aligned} \tag{19}$$

Substituting (17) into (19), as in (20), shown at the bottom of the next page.

p_i and q_i ($p_i > q_i$) are known to be positive and odd numbers, and $1 < p_i/q_i < 2$, then $0 < p_i/q_i\text{-}1 < 1$, also because $\sigma > 0$, then $e_{v_i}^{\frac{p_i}{q_i}-1} > 0$ ($e_{v_i} \neq 0$).

$$S_i\dot{S}_i = -\frac{p_i}{q_i}e_{v_i}^{\frac{p_i}{q}-1}\sigma\,|s| \le 0 \tag{21}$$

Visible, when $e_{v_i} \neq 0$, the system can reach the specified sliding plane in a limited time.

B. UPDATE CONTROL LAW

In order to approximate the random and non-linear disturbance caused by high-speed train operation and improve the robustness of the system, a double-loop recursive neural network(DLRNN) is introduced in this paper. DLRNN has strong nonlinear function approxima-tion ability [32]. Compared with the traditional Kalman filter method, it has better state variable estimation accuracy and faster convergence speed [33] and is suitable for the high-speed train dynamics model with strong nonlinear disturbance established in this paper. As shown in Figure 3, it uses internal and external loops to provide feedback signals and has higher approximation accuracy and convergence speed [34] than the single-loop feedback of traditional cyclic neural networks. In addition, in order to improve the adaptability of the neural network, a dynamic function is established and the update rule of the parameters is given.

(1) Nodes in the input layer are responsible for receiving input signals and sending them along with previous outputs to each node in the next layer, which can be represented as:

$$\theta_m = x_m \cdot W_{rom} \cdot exY_m \tag{22}$$

where x_m represents the input signal, W_{rom} represents the external feedback gain, and exY_m represents the previous output of the network.

(2) Nodes in the hidden layer not only use the signals transmitted by the input layer but also feedback on the results of the calculation of the Gaussian function to the input of the layer. For the ith node h_i:

$$h_i = \exp\left[-\frac{\|\theta_i \times r_i \cdot exh_i - c_i\|^2}{b_{\mathrm{i}}^2}\right] \tag{23}$$

c_i and b_{i} represent the center mean and standard deviation of the Gaussian function, respectively, and exh_i represent the result before the Gaussian function. r_i is the internal feedback gain.

(3) Each node in the output layer calculates the sum of all input signals as the output of the network as follows:

$$Y = \sum_{\mathrm{k}=1}^{n} W_k \mathrm{h}_k = W_1h_1 + W_2h_2 + \ldots + W_nh_n \tag{24}$$

where W_k is the weight value.

Because the system parameters of uncertainty are difficult to measure in practice, DLRNN is used to approximate the

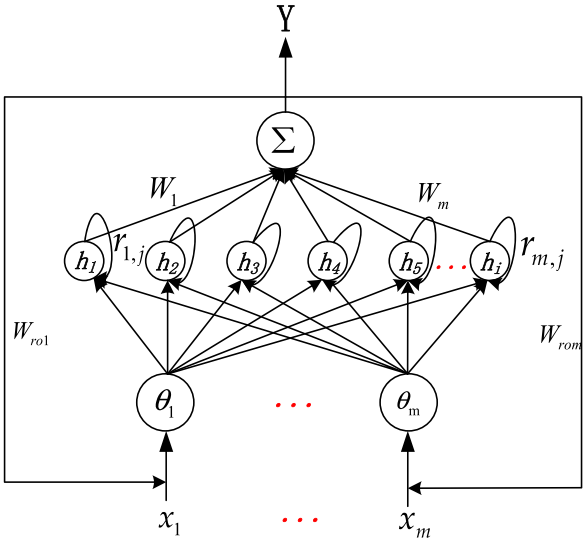

FIGURE 3. Diagram of a double-loop recursive neural network (DLRNN).

centralized uncertainty online. Suppose that high-speed train tracking error e_x and its derivative e_v are inputs of a double-loop recursive neural network. Centralized uncertainty can be simulated linearly with approximation error ε_i:

$$f_i = \mathbf{W}_i^{*T} I_i^* \left(\mathbf{x}_i, \mathbf{c}_i^*, \mathbf{b}_i^*, \mathbf{r}_i^*, W_{r0i}^*\right) + \varepsilon_i \tag{25}$$

where $\mathbf{x}_i$ is the input, $\mathbf{W}_i^*$ is the best weight vector, and $\mathbf{l}_i$ is the best base function vector.

The DLRNN used by the fractional order nonsingular terminal slider is represented as:

$$\hat{f}_i = \hat{\mathbf{W}}_i^T \hat{I}_i \left(\mathbf{x}_i, \hat{\mathbf{c}}_i, \hat{\mathbf{b}}_i, \hat{\mathbf{r}}_i, \hat{W}_{r0i}\right) \tag{26}$$

$\hat{\mathbf{W}}_i$ is an adjustable weight and $\hat{I}_i$ is the estimate of the best basis function.

The deviation between the function vector and its estimate is:

$$\begin{aligned}
\widetilde{I}_i &= I_{\mathrm{i}}^* - \hat{I}_{\mathbf{i}} \\
&= \left.\frac{\partial I_i}{\partial \mathbf{c}_i}\right|_{\mathbf{c}_i=\hat{\mathbf{c}}_i} \left(\mathbf{c}_i^* - \widehat{\mathbf{c}}_i\right) + \left.\frac{\partial I_i}{\partial \mathbf{b}_i}\right|_{\mathbf{b}_i=\hat{\mathbf{b}}_i} \left(\mathbf{b}_i^* - \widehat{\mathbf{b}}_i\right) \\
&\quad + \left.\frac{\partial I_i}{\partial \mathbf{r}_i}\right|_{\mathbf{r}_i=\hat{\mathbf{r}}_i} \left(\mathbf{r}_i^* - \widehat{\mathbf{r}}_i\right) + \left.\frac{\partial I_i}{\partial W_{roi}}\right|_{W_{ro}=\hat{W}_{ro}} \\
&\quad \times \left(W_{ro_i}^* - \hat{W}_{ro_i}\right) + O_{hi} \\
&= I_{i\mathbf{c}_i} \cdot \widetilde{\mathbf{c}}_i + I_{i\mathbf{b}_i} \cdot \widetilde{\mathbf{b}}_i + I_{ir_i} \cdot \widetilde{\mathbf{r}}_i + I_{iWro_i} \cdot \tilde{W}_{ro_i} + \mathbf{O}_{hi}
\end{aligned} \tag{27}$$

$\mathbf{O}_{hi}$ is the high-order error.

The centralized uncertainty approximation error is constructed as:

$$\begin{aligned}
\hat{f}_i - f_i &= \hat{\mathbf{W}}_{\mathbf{i}}^{\mathrm{T}} \hat{I}_{\mathrm{i}} - \mathbf{W}_{\mathbf{i}}^{*\mathrm{T}} I_{\mathrm{i}}^* - \varepsilon_i \\
&= \hat{\mathbf{W}}_{\mathbf{i}}^{\mathrm{T}} \hat{I}_{\mathrm{i}} - \left(\hat{\mathbf{W}}_{\mathbf{i}}^{\mathrm{T}} - \tilde{\mathbf{W}}_{\mathbf{i}}^{\mathrm{T}}\right) \left(\hat{I}_i - \tilde{I}_i\right) - \varepsilon_i \\
&= \tilde{\mathbf{W}}_{\mathbf{i}}^{\mathrm{T}} \hat{I}_{\mathrm{i}} + \hat{\mathbf{W}}_{\mathbf{i}}^{\mathrm{T}} \tilde{I}_i - \varepsilon_{0i}
\end{aligned} \tag{28}$$

where $\varepsilon_{0i} = \tilde{\mathbf{W}}_{\mathrm{i}}^{\mathrm{T}} \tilde{I}_{\mathbf{i}} + \varepsilon_i$

Using the DLRNN, the control law can be represented as:

$$\begin{aligned}
u_i(t) = \frac{\beta_i}{\xi \lambda_j} &\left[\sigma sgn(s) + \frac{q_i}{p_i} e_{v_i}^{2-\frac{p_i}{q_i}}(t) + \frac{q_i}{p_i} D^{\alpha} e_{v_i}^{2-\frac{p_i}{q_i}}(t)\right] \\
&+ \frac{\dot{v}_{d_i}(t)}{\xi \lambda_j} + \frac{1}{\lambda_j} \hat{f}_i(t)
\end{aligned} \tag{29}$$

To update the weights and functions of the DLRNN, the following update rules are designed:

$$\begin{cases}
\hat{\mathbf{W}}_i^T \mathbf{I}_{i_e} \dot{\hat{\mathbf{b}}}_i^T = \eta_{3i} \dfrac{1}{\beta_i} \dfrac{p_i}{q_i} \dot{e}_i^{p_i/q_i - 1} s_i \\
\hat{\mathbf{W}}_i^T \mathbf{I}_{i_{\mathrm{b}}} \dot{\hat{\mathbf{r}}}_i^T = \eta_{4i} \dfrac{1}{\beta_i} \dfrac{p_i}{q_i} \dot{e}_i^{p_i/q_i - 1} s_i \\
\hat{\mathbf{W}}_i^T \mathbf{I}_{i_r} \dot{\hat{W}}_{roi} = \eta_{5i} \dfrac{1}{\beta_i} \dfrac{p_i}{q_i} \dot{e}_i^{p_i/q_i - 1} s_i \hat{\mathbf{W}}_i^T \mathbf{I}_{i_{Wro}} \\
\dot{\hat{\mathbf{c}}}_i^T = \eta_{2i} \dfrac{1}{\beta_i} \dfrac{p_i}{q_i} \dot{e}_i^{p_i/q_i - 1} s_i
\end{cases} \tag{30}$$

$$\begin{aligned}
\dot{V} &= S_i \times \left[e_{v_i}(t) + \beta_i^{-1} \frac{p}{q} e_{v_i}^{\frac{p}{q}-1} \dot{e_{v_i}} + D^{\alpha} e_{v_i}\right] \\
&= S_i \times \left\{\begin{array}{l} e_{v_i}(t) + \beta_i^{-1} \frac{p}{q} e_{v_i}^{\frac{p}{q}-1} \times \\ \xi \left[- \left(\begin{array}{l} \frac{\beta_i}{\lambda_j \xi} \left[\sigma sgn(s) + \frac{q_i}{p_i} e_{v_i}^{2-\frac{p_i}{q_i}}(t) + \frac{q_i}{p_i} D^{\alpha} e_{v_i}^{2-\frac{p_i}{q_i}}(t)\right] \\ + \frac{\dot{v}_{d_i}(t)}{\lambda_j \xi} + \frac{1}{\lambda_j} f_i(t) \end{array} \right) \right] \\ + f_i(t) + D^{\alpha} e_{v_i}(t) \end{array}\right\} \\
&= \mathrm{S}_i \times \left[e_{v_i}(t) - \frac{p_i}{q_i} e_{v_i}^{\frac{p_i}{q_i}-1} \sigma sgn(s) - e_{v_i}(t) - D^{\alpha} e_{v_i}(t) + D^{\alpha} e_{v_i}(t)\right] \\
&= -\mathrm{S}_i \times \frac{p_i}{q_i} e_{v_i}^{\frac{p_i}{q_i}-1} \sigma sgn(s) \\
&= -\frac{p_i}{q_i} e_{v_i}^{\frac{p_i}{q_i}-1} \sigma \, |s|
\end{aligned} \tag{20}$$

Assumption 1 ([35]): During the learning process, the weight matrix $\left\|W_k^L\right\|(k = 0, 1, 2\cdots)$ is bounded. There exists a bo-unded open set $\Omega \subset \Re^{q\times(p+q)}$, such that $\{W_k\} \subset \Omega(k \in Z)$.

Remark 1: The activation function of the recurrent neural network and its derivatives of all orders are uniformly bounded on R. Therefore, assumption 1 is reasonable. In order to ensure the convergence of the iterative process, the conclusions in reference [35] are cited to ensure the strong convergence of the recurrent neural network.

C. PROOF OF STABILITY

Select the following Lyapunov function:

$$V = \frac{1}{2}s_i^2 + \frac{1}{2\eta_{1i}}\mathrm{tr}\left(\tilde{\mathbf{W}}_i^T\tilde{\mathbf{W}}_i\right) + \frac{1}{2\eta_{2i}}\mathrm{tr}\left(\tilde{\mathbf{c}}_i^T\tilde{\mathbf{c}}_i\right) + \frac{1}{2\eta_{3i}}\mathrm{tr}\left(\tilde{\mathbf{b}}_i^T\tilde{\mathbf{b}}_i\right) + \frac{1}{2\eta_{4i}}\mathrm{tr}\left(\tilde{\mathbf{r}}_i^T\tilde{\mathbf{r}}_i\right) + \frac{1}{2\eta_{5i}}\tilde{W}_{roi}^2 \quad (31)$$

We define:

$$N_i = \frac{1}{2\eta_{1i}}\mathrm{tr}\left(\tilde{\mathbf{W}}_i^T\tilde{\mathbf{W}}_i\right) + \frac{1}{2\eta_{2i}}\mathrm{tr}\left(\tilde{\mathbf{c}}_i^T\tilde{\mathbf{c}}\right) + \frac{1}{2\eta_{3i}}\mathrm{tr}\left(\tilde{\mathbf{b}}_i^T\tilde{\mathbf{b}}\right) + \frac{1}{2\eta_{4i}}\mathrm{tr}\left(\tilde{\mathbf{r}}_i^T\tilde{\mathbf{r}}_i\right) + \frac{1}{2\eta_{5i}}\tilde{W}_{roi}^2 \quad (32)$$

By making a time differential of V and substituting (30) and (32), the following results can be obtained:

$$\begin{aligned}\dot{V} &= s_i\dot{s}_i + \dot{N}_i \\ &= -\frac{1}{\beta_i}\frac{p_i}{q_i}\dot{e}_{vi}^{\frac{p_i}{q_i}-1}s_i\left[\hat{f}_i - f_i + \sigma\,\mathrm{sgn}\,(s_i)\right] + \dot{N}_i\end{aligned} \quad (33)$$

Substituting (28) into (33):

$$\begin{aligned}\dot{V} &= s_i\dot{s}_i + \dot{N}_i \\ &= -\frac{1}{\beta_i}\frac{p_i}{q_i}\dot{e}_{vi}^{\frac{p_i}{q_i}-1}s_i\begin{bmatrix}\hat{\mathbf{W}}_{\mathbf{i}}^{\mathrm{T}}\hat{I}_{\mathrm{i}} - \mathbf{W}_i^{*T}I_{\mathrm{i}}^* \\ -\varepsilon_i + \sigma\,\mathrm{sgn}\,(s_i)\end{bmatrix} + \dot{N}_i\end{aligned} \quad (34)$$

By substituting (27) and the law of renewal (28) into (34):

$$\begin{aligned}\dot{V} = &-\frac{1}{\beta_i}\frac{p_i}{q_i}\dot{e}_i^{p_i/q_i-1}s_i\tilde{\mathbf{W}}_i^T\hat{\mathbf{I}} \\ &-\frac{1}{\beta_i}\frac{p_i}{q_i}\dot{e}_i^{p_i/q_i-1}s_i\hat{\mathbf{W}}_i^T \\ &\times\left(\mathbf{I}_{i_c}\tilde{\mathbf{c}}_i + \mathbf{I}_{i_b}\tilde{\mathbf{b}}_i + \mathbf{I}_{i_r}\tilde{\mathbf{r}}_i + \mathbf{I}_{iW_{ro}}\tilde{W}_{\mathrm{roi}} + \mathbf{O}_{hi}\right) \\ &-\frac{1}{\beta_i}\frac{p_i}{q_i}\dot{e}_i^{p_i/q_i-1}s_i\left[(\sigma\ \ \mathrm{sgn}\,(s_i) - \varepsilon_i\right] \\ &+\frac{1}{\eta_{1i}}\mathrm{tr}\left(\tilde{\mathbf{W}}^T\dot{\tilde{\mathbf{W}}}\right) + \frac{1}{\eta_{2i}}\mathrm{tr}\left(\dot{\tilde{\mathbf{c}}}^T\tilde{\mathbf{c}}\right) \\ &+\frac{1}{\eta_{3i}}\mathrm{tr}\left(\dot{\tilde{\mathbf{b}}}^T\tilde{\mathbf{b}}\right) + \frac{1}{\eta_{4i}}\mathrm{tr}\left(\dot{\mathbf{r}}^T\tilde{\mathbf{r}}\right) + \frac{1}{\eta_{5i}}\left(\dot{\tilde{W}}_{ro}\tilde{W}_{ro}\right)\end{aligned} \quad (35)$$

Substituting the updated law (30) into (35) yields:

$$\begin{aligned}\dot{V} &= -\frac{1}{\beta_i}\frac{p_i}{q_i}\dot{e}_i^{p_i/q_i-1}s_i\left[\sigma\,\mathrm{sgn}\,(s_i) - \varepsilon_i + O_{h0i}\right] \\ &= -\frac{1}{\beta_i}\frac{p_i}{q_i}\dot{e}_i^{p_i/q_i-1}s_i\sigma\,\mathrm{sgn}\,(s_i) - \frac{1}{\beta_i}\frac{p_i}{q_i}\dot{e}_i^{p_i/q_i-1}s_i(O_{h0i} - \varepsilon_i) \\ &\le -\frac{1}{\beta_i}\frac{p_i}{q_i}\dot{e}_i^{p_i/q_i-1}|s_i|\,\sigma - \frac{1}{\beta_i}\frac{p_i}{q_i}\dot{e}_i^{p_i/q_i-1}|s_i|\,(O_{h0i} - \varepsilon_i)\end{aligned} \quad (36)$$

where $O_{h0i} = \hat{\mathbf{W}}_i^T\mathbf{O}_{hi}$

Assumption 2: There are unknown constant numbers ε_{ui} and O_{ui} that satisfy the $|\varepsilon_i| \le \varepsilon_{ui}$ and $|O_{h0i}| \le O_{ui}$ bounded conditions.

Remark 2: For fractional order linear system with parameter perturbation of system variables, given parameter vector β, where $\beta = (\beta_1, \beta_2, \cdots \beta_q) \in \mathbb{R}^q$, the corresponding system is defined as S_β. If parameter β makes system S_β asymptotically stable, then parameter β is the system stability parameter of system S_β. The set of all system stability parameters is called the stable parameter region marked as F_β. The sufficient and necessary condition for asymptotic stability of fractional order linear system with parameter perturbations is that all parameters in the system matrix of parameter perturbations are in the stable parameter region F_β.

If a suitable value of O_{h0i} is selected such that $O_{h0i} > \varepsilon_i$ and $\sigma > 0$ at the same time, then $\dot{V} < 0$ can be obtained. $\dot{V}$ is semi-negative definite, indicating that both $\tilde{\mathbf{c}}_i, \tilde{\mathbf{b}}_i, \tilde{\mathbf{r}}_i, \tilde{W}_{\mathrm{roi}}$ and $\hat{\mathbf{W}}_i$ are bounded. It can be concluded from (14) that $\dot{S}_i$ is also bounded.

Integral over (36):

$$\begin{aligned}&\int_0^t \frac{1}{\beta_i}\frac{p_i}{q_i}\dot{e}_i^{p_i/q_i-1}|s_i|\,\sigma\,dt + \int_0^t \frac{p_i}{q_i}\dot{e}_i^{p_i/q_i-1}|s_i|\,(O_{h0i} - \varepsilon_i)dt \\ &\le V(0) - V(t)\end{aligned} \quad (37)$$

Since $V_i(0)$ is bounded, $V_i(t)$ is bounded and not increasing, $\int_0^t \frac{1}{\beta_i}\frac{p_i}{q_i}\dot{e}_i^{p_i/q_i-1}|s_i|\,\sigma\,dt$ and $\int_0^t \frac{p_i}{q_i}\dot{e}_i^{p_i/q_i-1}|s_i|\,(O_{h0i} - \varepsilon_i)$ are bounded, the tracking error will converge to zero asymptotically and the system will have asymptotic stability according to the Barbarat's lemma [36].

D. IMPROVED GREY WOLF OPTIMIZATION ALGORITHM

The objective of control system optimization in this paper is to obtain the optimal parameters for the FONFTSM controller and DLRNN interference approximation. The GWO is an optimization algorithm that simulates the strict social hierarchy mechanism and hunting behavior of the grey wolf population. It has the advantages of few adjustment parameters, simple principles, easy implementation, and adjustable adaptive convergence factor. It has been widely used in solving various optimization problems [37]. However, the general GWO algorithm has the drawbacks of low convergence accuracy and poor global search ability. For this reason, an improved GWO(IGWO) algorithm with a non-linear convergence factor and inertial weight factor is designed to improve the convergence speed and accuracy of the algorithm.

1) GENERAL GWO ALGORITHM

To simulate the search rank of gray wolves, the preferences are Gray Wolf α, Gray Wolf β, and Gray Wolf δ, and the rest are Gray Wolf ω.

During the hunting process, when the location of the prey is determined, the gray wolf population encloses the prey according to the following formula:

$$\vec{D} = \left|\vec{C} \cdot \vec{X}_p(t) - \vec{X}(t)\right|$$
$$\vec{X}(t+1) = \vec{X}_p(t) - \vec{A} \cdot \vec{D} \tag{38}$$

$\vec{X}(t)$ is the current location of the gray wolf, $\vec{X}_P(t)$ is the current location of the prey, $\vec{D}$ is the distance between the individual and the prey, $\vec{X}(t+1)$ is the updated location of the gray wolf, $\vec{A}$ and $\vec{C}$ are the coefficient vectors, then:

$$\vec{a} = 2 - 2t/T_{\max}$$
$$\vec{A} = 2\vec{a} \cdot \vec{r}_1 - \vec{a}$$
$$\vec{C} = 2\vec{r}_2 \tag{39}$$

where $\vec{a}$ is the convergence factor that decreases linearly from 2 to 0 with the number of iterations t, $T_{\max}$ is the maximum number of iterations, $\vec{r}_1$ and $\vec{r}_2$ are random vectors between each component [0,1].

During the hunting process, gray wolf α usually identifies the location of the prey, and leads gray wolf β and δ to guide the entire gray wolf population around the prey. The individual wolves are updated according to the following:

$$\vec{D}_\alpha = \left|\vec{C}_1 \cdot \vec{X}_\alpha(t) - \vec{X}(t)\right|, \vec{X}_1 = \vec{X}_\alpha(t) - \vec{A}_1 \cdot \left(\vec{D}_\alpha\right)$$
$$\vec{D}_\beta = \left|\vec{C}_2 \cdot \vec{X}_\beta(t) - \vec{X}(t)\right|, \vec{X}_2 = \vec{X}_\beta(t) - \vec{A}_2 \cdot \left(\vec{D}_\beta\right)$$
$$\vec{D}_\delta = \left|\vec{C}_3 \cdot \vec{X}_\delta(t) - \vec{X}(t)\right|, \vec{X}_3 = \vec{X}_\delta(t) - \vec{A}_3 \cdot \left(\vec{D}_\delta\right)$$
$$\vec{X}(t+1) = \frac{\left(\vec{X}_1 + \vec{X}_2 + \vec{X}_3\right)}{3} \tag{40}$$

Among them, $\vec{D}_\alpha, \vec{D}_\beta, \vec{D}_\delta$ represent the current distances between gray wolf and gray wolf α, gray wolf β and gray wolf δ, $\vec{X}_\alpha, \vec{X}_\beta, \vec{X}_\delta$ represents the locations of gray wolf α, β and δ, and $\vec{X}_1, \vec{X}_2, \vec{X}_3$ represent the locations of gray wolf α, β and δ after disturbance, respectively. Figure 4 shows the iterative process of the grey wolf optimization algorithm

2) IMPROVED GREY WOLF OPTIMIZATION ALGORITHM

The GWO algorithm has poor searchability and is prone to fall into local optimum when solving some optimization problems. Therefore, its convergence factor $\vec{a}$ is nonlinearized, and the conversion of the convergence factor from linear to exponential form improves the convergence speed of the algorithm. $\vec{a}$ is designed as:

$$\vec{a} = 2e^{-\left(\frac{4t}{T_{\max}}\right)^2} \tag{41}$$

After the non-linearization of the convergence factor $\vec{a}$ according to the (41), the convergence factor decreases faster

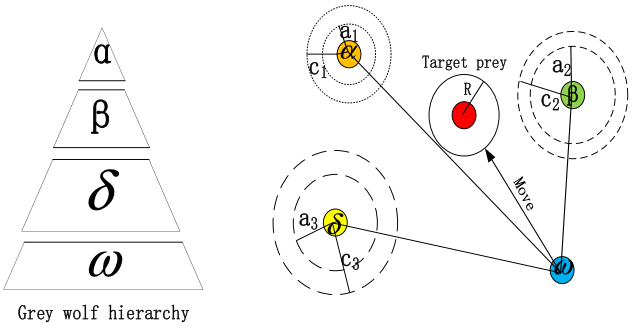

FIGURE 4. Gray Wolf algorithm execution.

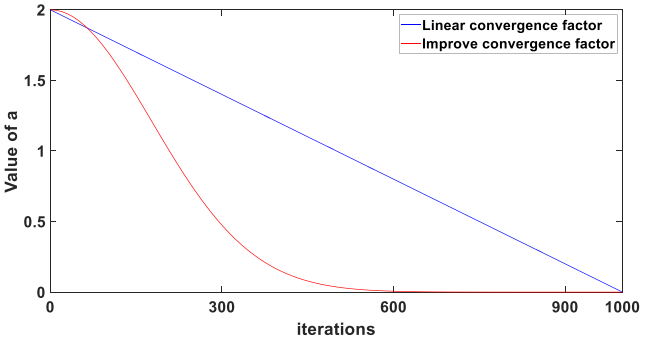

FIGURE 5. Convergence factor with a number of iterations.

in the early search period, which is helpful to speed up the global search, While it decreases slowly in the late iteration period, which is helpful for full local search. Figure 5 shows the comparison of iterations after the nonlinearization of the convergence factor with those before it is processed.

In the GWO algorithm, the first three levels of the gray wolf $\vec{X}_\alpha, \vec{X}_\beta, \vec{X}_\delta$ guide the entire gray wolf population for location updates, and the weight is one-third, which can not fully reflect the guiding position of different levels of the gray wolf. Therefore, the inertial weighting strategy is introduced into the GWO algorithm, which makes the higher-level wolves have larger inertial weights and speeds up the convergence of the algorithm. Moreover, in order to further improve the accuracy of the GWO algorithm, the position of the first three classes of gray wolves is calculated differently from that of the disturbed wolves, and a new location update algorithm is designed as:

$$\vec{W}_1 = \left|\vec{X}_1\right| / \left(\left|\vec{X}_1\right| + \left|\vec{X}_2\right| + \left|\vec{X}_3\right|\right)$$
$$\vec{W}_2 = \left|\vec{X}_2\right| / \left(\left|\vec{X}_1\right| + \left|\vec{X}_2\right| + \left|\vec{X}_3\right|\right)$$
$$\vec{W}_3 = \left|\vec{X}_3\right| / \left(\left|\vec{X}_1\right| + \left|\vec{X}_2\right| + \left|\vec{X}_3\right|\right)$$
$$\vec{X}'(t) = \vec{W}_1 \cdot \left(\vec{X}_1 - \vec{X}_\alpha\right) + \vec{W}_2 \cdot \left(\vec{X}_2 - \vec{X}_\beta\right) + \vec{W}_3 \cdot \left(\vec{X}_3 - \vec{X}_\delta\right) \tag{42}$$

The introduction of a greedy selection strategy can effectively improve the solution accuracy of the GWO algorithm and enhance the local search ability. The specific operations

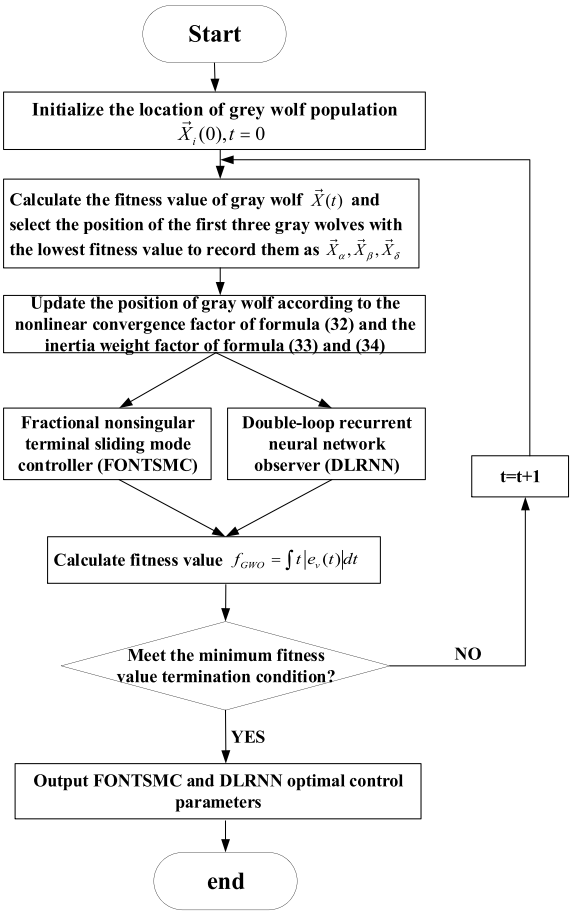

FIGURE 6. IGWO parameter optimization process.

are as follows: if $f\left(\vec{X}'(t)\right) < f(\vec{X}(t))$, $\vec{X}(t+1) = \vec{X}'(t)$, otherwise $\vec{X}(t+1) = \vec{X}(t)$, $f(\vec{X}(t))$ is the gray wolf's fitness function.

For this system, select the ITAE function that defines the performance criteria of the target function as the evaluation function. The fitness evaluation function of the algorithm is selected as follows:

$$f_{GWO} = \int t\,|e_v(t)|dt \tag{43}$$

$e_v(t)$ is the train speed tracking error, which minimizes the objective function to obtain the best speed tracking accuracy and convergence speed.

The execution flow of the improved grey wolf optimization parameter optimization algorithm is shown in Figure 6:

As shown in Figure 6, the parameters of the IGWO algorithm are initialized first, and the first three gray wolf locations with the smallest suitability value are selected to be the best locations of the three $\vec{X}_\alpha, \vec{X}_\beta, \vec{X}_\delta$ wolves. Then the location of the gray wolf is updated with the nonlinearization of the gray wolf population convergence factor and the addition of the inertial weight factor. The location information is then substituted into the FONTSMC controller and the DLRNN observer, respectively, to compute the fitness evaluation function. Finally, if the calculated fitness does not meet the end condition, the gray wolf position will be recalculated and modified by the location update strategy. If the fitness value meets the end condition, the optimal control parameter will be output and the algorithm iteration ends.

TABLE 1. Controller parameters.

parameter	parameter values	Company
a_{0i}(t)	a_{0i}(t)∈[0.50,0.60]	N/kg
a_{1i}(t)	a_{1i}(t)∈[0.0035,0.0045]	N·s/m·kg
a_{2i}(t)	a_{2i}(t)∈[0.000110,0.0001180]	N·s^2/m^2·kg
λ_{in}	λ_{i1}=0.94,λ_{i2}=0.91,λ_{i3}=0.85,λ_{i4}=0.80	—
θ_i(t)	θ_i(t)=[(π*rand)/180]	◦
R_i(t)	R_i(t)∈[5,6]	km
L_i(t)	L_i(t)∈[4,4.3]	km
β_i^{-1}	β_1^{-1}=1,β_2^{-1}=1.05,β_3^{-1}=0.95,β_4^{-1}=1.08	—
σ_i	σ_1=0.05,σ_2=0.06,σ_3=0.02,σ_4=0.05	—
η_{1i}	η_{11} =0.89, η_{12} =0.98, η_{13} =1.20, η_{14} =1.20	—
η_{2i}	η_{21} =1.15, η_{22} =1.31, η_{23} =0.97, η_{24} =1.65	—
η_{3i}	η_{31} =0.75, η_{32} =1.52, η_{33} =1.33, η_{34} =0.76	—
η_{4i}	η_{41} =1.28, η_{42} =1.45, η_{43} =0.88, η_{44} =1.10	—
η_{5i}	η_{51} =1.74, η_{52} =0.95, η_{53} =1.48, η_{54} =1.65	—
p_i	p_1=p_2=p_3=p_4=5	—
q_i	q_1=q_2=q_3=q_4=3	—
α_i	$\alpha_1=\alpha_2=\alpha_3=\alpha_4$ =0.5,	—
w_i(0)	w_1(0)=[-0.7162 -0.1565 0.8315 0.5844 0.9190 0.3115 -0.9286 0.6983 0.8680 0.3575 0.5155 0.4863 -0.2155 0.3110 -0.6576] w_2(0)=[0.4121 -0.9363 -0.4462 -0.9077 -0.8057 0.6469 0.3897 -0.3658 0.9004 -0.9311 -0.1225 -0.2369 0.5310 0.5904 -0.6263] w_3(0)=[0.5025 -0.4898 0.0119 0.3982 0.7818 0.9186 0.0944 -0.7228 -0.7014 -0.4850 0.6814 -0.4914 0.6286 -0.5130 0.8585] w_4(0)=[-0.8483 -0.8921 0.0616 0.5583 0.8680 -0.7402 0.1376 -0.0612 -0.9762 -0.3258 -0.6756 0.5886 -0.3776 0.0571 -0.6687]	—

IV. SIMULATION ANALYSIS

In order to analyze the performance of the fractional order nonsingular terminal sliding mode control method mentioned above, four CRH5 series trains are selected as the controlled objects. The reference input speed of the simulation is the actual traction braking and idle running curves of the train. The maximum running speed is 350 km/h, and it enters the working conditions of ramps, curves, and tunnels in different time periods. The total weight of the train is 400 tons, the length of the train is 211.5m, and the rotation mass factor

is 0.06 [38]. The sampling period is set to 64 ms, and the uncertain parameters of the control system are derived from the IGWO algorithm as shown in Table 1. There are a total of 32 parameters that need to be optimized, mainly including control system parameters β_i^{-1}, σ_i and the DLRNN parameters $w(0)$, η. The outer ring gain $w_{\mathrm{roi}}(0)$ and inner ring gain $r_{\mathrm{i}}(0)$ of DLRNN are chosen as 15 (0,1) random numbers.

The expected target speed curve for the actual operation of high-speed trains is designed as in (44), which includes seven stages: 0s < t ⩽ 16s and 38.4s < t ⩽ 76.8s are acceleration stages,16s < t ⩽ 38.4s,76.8s < t ⩽ 105.6s and 128s < t ⩽ 153.6s are constant speed operation stages, and 105.6s < t ⩽ 128s and 153.6s < t ⩽ 200s are braking stages.

$$\begin{cases} -\left(250/16^2\right) \times (t-16)^2 + 250, \; t \le 16s \\ 250, \; 16s < t \le 38.4s \\ -\left(400/76.8^2\right) \times (t-76.8)^2 + 350, \\ 38.4s < t \le 76.8s \\ 350, \; 76.8s < t \le 105.6s \\ -\left(150/22.4^2\right) \times (t-105.6)^2 + 350, \\ \quad 105.6s < t \le 128s \\ 200, \; 128s < t \le 153.6s \\ -\left(200/46.4^2\right) \times (t-153.6)^2 + 200, \\ \quad 153.6s < t \le 200s \end{cases} \tag{44}$$

Designing actuator failure factors that vary over time to simulate possible actuator failures during high-speed train operation. Described as (45):

$$\lambda_i(t) = \begin{cases} 1, & t < 12.8s \\ 0.85 + 0.1\sin(0.2t), & 12.8s \le t < 76.8s \\ 0.86 + 0.1\cos(0.3t), & 76.8s \le t < 128s \\ 0.87 + 0.1e^{-0.1t}, & t \ge 128s \end{cases} \tag{45}$$

A. PERFORMANCE ANALYSIS OF THE IMPROVED GREY WOLF OPTIMIZATION ALGORITHM

In order to verify the advantages of the IGWO in this paper, selecting the traditional GWO and PSO to compare with the proposed method. Figure 7 shows the convergence comparison between the IGWO algorithm, GWO algorithm, and PSO algorithm.

Figure 7 shows that IGWO is superior to the original GWO and the PSO in global convergence speed and accuracy, and can accurately and quickly derive the controller's uncertain parameter values.

B. SIMULATION ANALYSIS OF CONTROL PERFORMANCE

Using equations (5)-(7) to calculate the minimum safe distance between high-speed trains. The initial distance between two adjacent trains is set to 2000 meters. In order to verify the effective control of the proposed method under the actual operating conditions of high-speed trains, introduced actuator failure factors that vary over time in (45). Figure 8 shows the

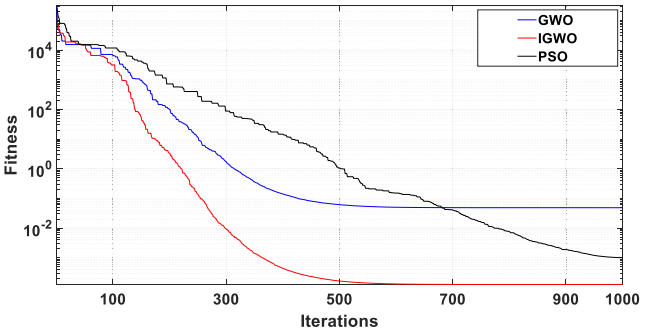

FIGURE 7. Comparison of improved algorithm with original algorithm and PSO algorithm.

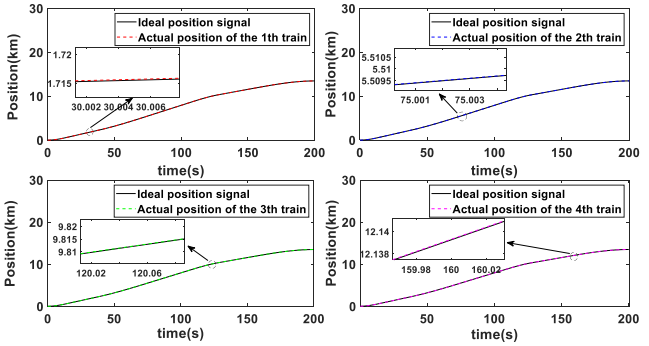

FIGURE 8. Displacement tracking curve.

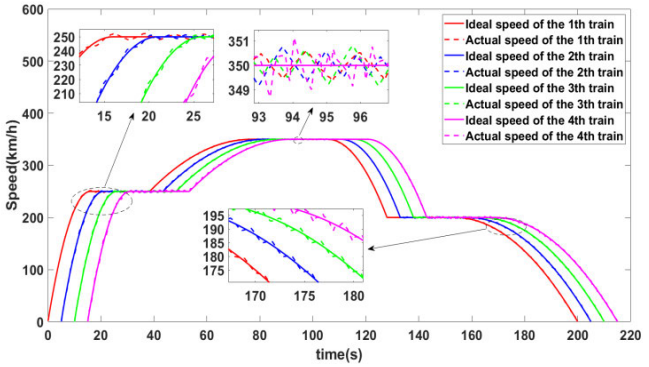

FIGURE 9. Speed tracking curve.

displacement tracking curve, Figure 9 shows the speed tracking curve, and Figure 10 shows the speed tracking error of high-speed trains, Figure 11 shows the control input changes for each train.

As can be seen from Figure 8 and Figure 9, the fractional order nonsingular terminal sliding mode controller designed in this paper can achieve accurate displacement and speed tracking for high-speed trains in the event of actuator failure. During the traction and braking stages of high-speed trains, it can better track the target's expected speed. When operating at a high speed of 350 km/h, it can also accurately track the expected speed, in addition to small jitter, within a reasonable error range.

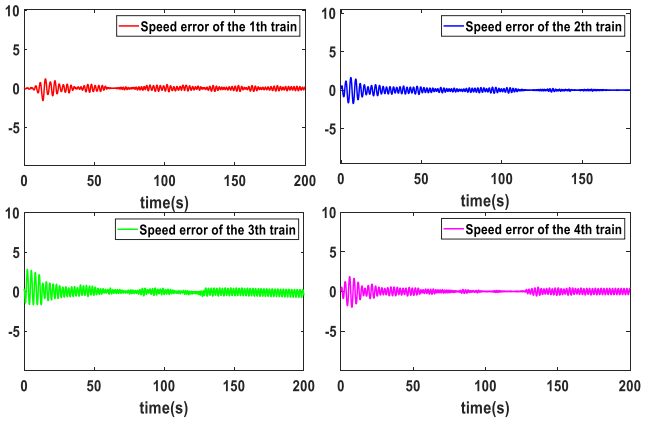

FIGURE 10. Speed tracking error.

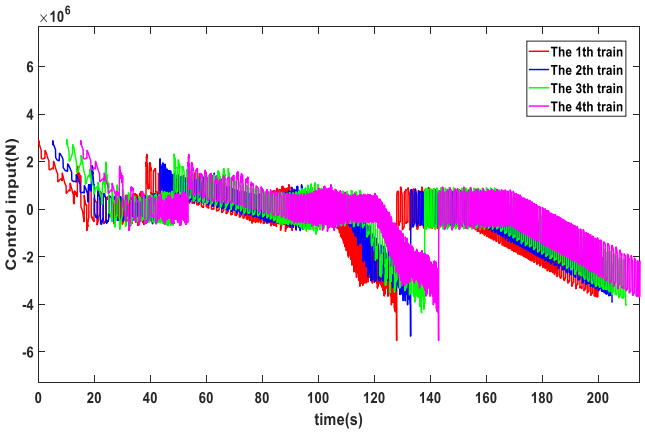

FIGURE 11. Train input control quantity.

The speed tracking error shown in Figure 10 indicates that in addition to relatively large errors during the startup phase, the method designed can enable the train to operate at an accurately controlled speed during other time periods. The input control quantity variation diagram in Figure 11 shows the stable input of the control quantity of the designed algorithm. In addition to the large range variation during startup, it can maintain stable variation and small range fluctuation during subsequent traction braking and constant speed operation, and the control effect is ideal.

Figure 12 shows the simulation diagram of the convergence of the sliding surface of each train. It can be concluded from the figure that under the method designed in this article, the sliding surface functions of each train converge to stable values within a finite time, with the time being 12.736s for the 1th train, 12.533s for the 2th train, 12.625s for the 3th train, and 12.708s for the 4th train.

In order to explore the impact of deviating from the nominal parameters of trains on speed and displacement tracking of high-speed trains, this paper takes deviating from the normal mass of trains as an example to obtain the mean speed tracking error(MSTE) and mean displacement tracking error(MDTE) of each train. As shown in Table 2.

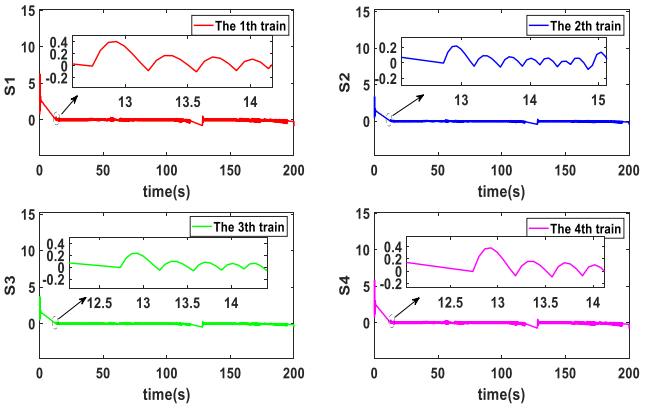

FIGURE 12. Convergence of sliding surface for each train.

TABLE 2. Statistics of train tracking error under deviation from nominal mass.

Train mass (tons)	index	The 1th	The 2th	The 3th	The 4th
385	MDTE (km)	2.253×10^{-5}	1.958×10^{-5}	2.054×10^{-5}	2.347×10^{-5}
	MSTE (km/h)	0.282	0.431	0.102	0.218
390	MDTE (km)	2.142×10^{-5}	2.332×10^{-5}	1.871×10^{-5}	1.995×10^{-5}
	MSTE (km/h)	0.305	0.285	0.351	0.248
395	MDTE (km)	1.856×10^{-5}	1.978×10^{-5}	2.532×10^{-5}	2.056×10^{-5}
	MSTE (km/h)	0.209	0.201	0.364	0.179
400	MDTE (km)	2.034×10^{-5}	2.155×10^{-5}	1.910×10^{-5}	2.187×10^{-5}
	MSTE (km/h)	0.311	0.435	0.347	0.146
405	MDTE (km)	2.245×10^{-5}	1.975×10^{-5}	2.013×10^{-5}	2.214×10^{-5}
	MSTE (km/h)	0.187	0.223	0.371	0.413
410	MDTE (km)	1.896×10^{-5}	2.148×10^{-5}	1.991×10^{-5}	2.145×10^{-5}
	MSTE (km/h)	0.317	0.265	0.460	0.207
415	MDTE (km)	1.894×10^{-5}	1.907×10^{-5}	2.301×10^{-5}	1.981×10^{-5}
	MSTE (km/h)	0.379	0.145	0.276	0.198

From Table 2, it can be seen that the method designed in this paper can maintain the mean displacement tracking error of each train below 2.4×10^{-5}(km) and the mean speed tracking error of each train below 0.5(km/h) when deviating from the standard mass of the train by 400±15 tons. The change in the nominal mass of the train has little impact on the control accuracy, and it also verifies the high accuracy

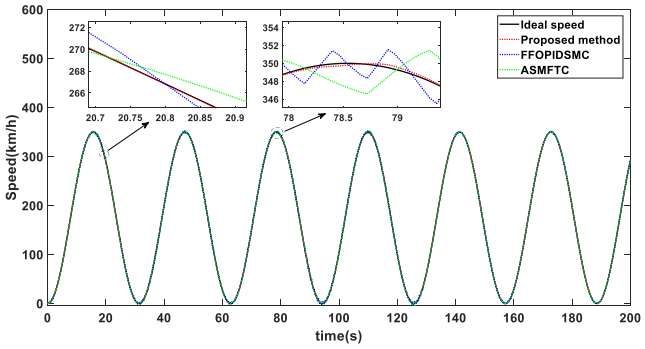

FIGURE 13. Velocity tracking when the input is a sine wave.

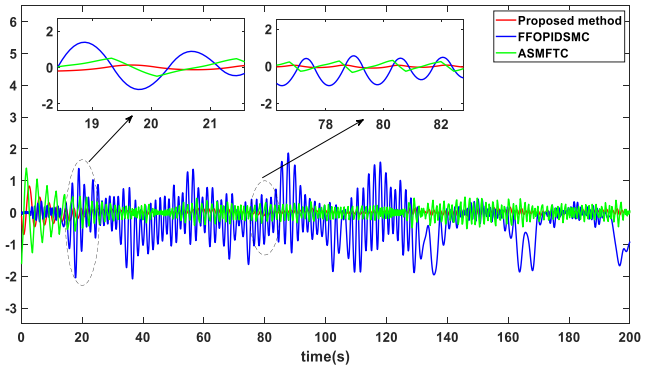

FIGURE 14. Velocity tracking error when the input is a sine wave.

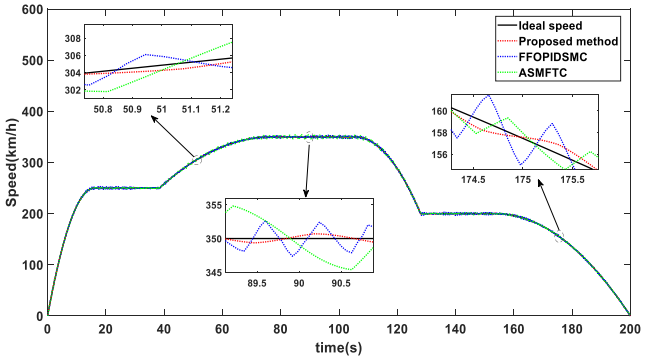

FIGURE 15. Speed tracking when input is actual operating conditions.

and stability of the control method designed in this paper when high-speed trains are fully loaded with passengers and unloaded.

C. COMPARE WITH OTHER METHODS

To validate the real-time tracking performance of the proposed method, two advanced control methods the fractional order PID sliding mode fault-tolerant control (FFOPIDSMC) [39] and the adaptive sliding mode fault-tolerant control (ASMFTC) [40] are selected to compare with the proposed method. Figure 13 and Figure 15 show the comparison results when the reference input is a sine wave and the actual operation curve, respectively; Figure 14 shows the tracking

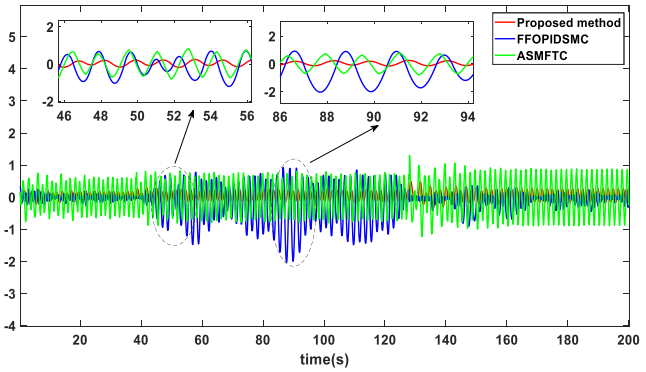

FIGURE 16. Speed tracking when input is actual operating conditions.

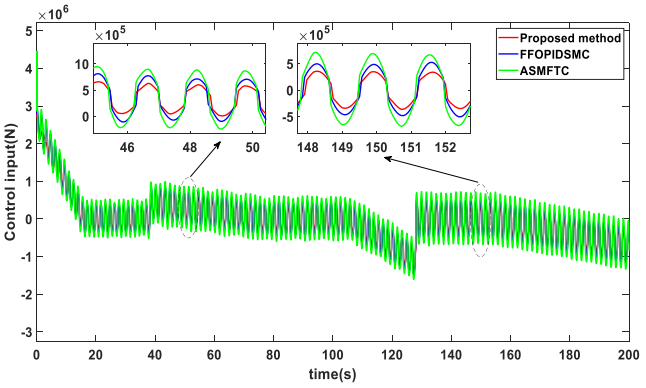

FIGURE 17. Three methods for controlling input changes.

error when the input is a sine wave, and Figure 16 shows the tracking error when the input is the actual operating condition; Figure 17 shows the input control quantity changes for the three control methods.

As shown in Figure 13 and Figure 15, the FFOPIDSMC and ASMFTC methods can also more accurately track the ideal input curve under the sine wave and actual operation tracking trajectory, but the chattering phenomenon is obvious, and the tracking effect in the uniform speed and acceleration/deceleration stages of train operation is not as good as the method proposed in this paper. Compared with the FFOPIDSMC and ASMFTC, the proposed method has a smoother speed tracking trajectory, higher tracking accuracy, and faster response speed.

As can be seen from Figures 14 and 16, the speed tracking error of the proposed method is significantly smaller than FFOPIDSMC and ASMFTC. The control system designed in this paper can accurately track expected signals under external random disturbances, and has low sensitivity to parameters, reflecting the robustness and stability of the method designed.

To verify the sensitivity of the designed algorithm to parameters and dynamic uncertainties, Monte Carlo global sensitivity analysis method is used for sensitivity analysis. The impact of these parameters changing within the value range on the control input, and tracking error root mean

TABLE 3. Comparative analysis of system sensitivity indicators.

Evaluation index		FFOPIDSMC	ASMFTC	Proposed method
$e(t)$	RMSE	0.1524	0.0787	0.0405
	MAE	0.0517	0.0343	0.0175
$\dot{e}(t)$	RMSE	1.1448	0.7178	0.2386
	MAE	0.1944	0.1016	0.0304
$u_i(t)$	RMSE	0.6255	0.8345	0.5508
	MAE	0.4658	0.5177	0.3796

square error(RMSE) and mean absolute error(MAE) value are obtained, as shown in Table 3.

From the data in Table 3, the tracking error of the proposed method and the RMSE and MAE values of the control signal are significantly lower than those of the FFOPIDSMC and ASMFTC methods. The position and speed tracking error under the actual operating condition has more ideal robustness and stability. It can meet the complex nonlinearity and time variation of high-speed trains.

The input control quantities of this method, fractional order PID sliding mode control, and adaptive fault-tolerant sliding mode control methods are shown in Figure 17. It can be seen that the control quantity vibration of the method proposed in this paper is significantly smaller than the vibration of the two methods. When a high-speed train fails, the control quantity can still be stably output, and the control quantity always remains within a reasonable vibration range. Compared with the FFOPIDSMC method and the ASMFTC method, the output control variables of the method proposed in this paper fluctuate less with time and have better control stability.

V. CONCLUSION

In this paper, a fractional order nonsingular terminal sliding mode control method with fast convergence in finite time and high sensitivity is proposed by introducing a distance potential function to accurately adjust the output size of the control variable according to the distance constraint of multi-train high-speed train interval. A double-loop recursive neural network is introduced to quickly approximate the uncertain external random disturbances during the operation of high-speed trains. A fault-tolerant control system with high robustness is established by updating the control parameters of the neural network online with adaptive law. The stability of the control system is proved by Lyapunov. For the uncertain parameters of the control system, an improved grey wolf optimization algorithm is proposed. By using the idea of inertial weight distribution and non-linearization of the convergence factor, the global search ability and local search speed of the optimization algorithm are enhanced, and the control accuracy of the algorithm is improved. The simulation results show that the method designed in this paper can track the ideal speed and displacement of high-speed trains quickly and accurately, Compared with other advanced control methods, the proposed method can converge to the balance point more quickly and has higher control accuracy and better robustness.

REFERENCES

[1] W. ShangGuan, X. Yan, B. Cai, and J. Wang, "Multiobjective optimization for train speed trajectory in CTCS high-speed railway with hybrid evolutionary algorithm," *IEEE Trans. Intell. Transp. Syst.*, vol. 16, no. 4, pp. 2215–2225, Aug. 2015.

[2] X. Wang, L. Zhu, H. Wang, T. Tang, and K. Li, "Robust distributed cruise control of multiple high-speed trains based on disturbance observer," *IEEE Trans. Intell. Transp. Syst.*, vol. 22, no. 1, pp. 267–279, Jan. 2021.

[3] D. Li, "Sliding mode adaptive robust H_∞ control method for high-speed train under strong wind conditions,," *J. China Railway Soc.*, vol. 40, no. 7, pp. 67–73, 2018.

[4] Y. Guo, P. Sun, X. Feng, and K. Yan, "Adaptive fuzzy sliding mode control for high-speed train using multi-body dynamics model," *IET Intell. Transp. Syst.*, vol. 17, no. 2, pp. 450–461, Sep. 2022.

[5] C. A. Monje, Y. Q. Chen, and B. M. Vinagre, *Fractional-Order Systems and Controls: Fundamentals and Applications*. Cham, Switzerland: Springer, 2010.

[6] S. Pashaei and F. Hashemzadeh, "A new fractional-order control method for robust synchronization between fractional-order uncertain permanent magnet synchronous motors," in *Proc. 27th Iranian Conf. Electr. Eng. (ICEE)*, Apr. 2019, pp. 904–908.

[7] H. Razmi and S. Afshinfar, "Neural network-based adaptive sliding mode control design for position and attitude control of a quadrotor UAV," *Aerosp. Sci. Technol.*, vol. 91, pp. 12–27, Aug. 2019.

[8] S. Song, B. Zhang, J. Xia, and Z. Zhang, "Adaptive backstepping hybrid fuzzy sliding mode control for uncertain fractional-order nonlinear systems based on finite-time scheme," *IEEE Trans. Syst. Man, Cybern. Syst.*, vol. 50, no. 4, pp. 1559–1569, Apr. 2020.

[9] J. Sabatier, P. Lanusse, P. Melchior, and A. Oustaloup, "Fractional order differentiation and robust control design," *Intell. Syst., Control Automat., Sci. Eng.*, vol. 77, pp. 13–18, Jan. 2015.

[10] T. Kaczorek, "Positive linear systems consisting of n subsystems with different fractional orders," *IEEE Trans. Circuits Syst. I, Reg. Papers*, vol. 58, no. 6, pp. 1203–1210, Jun. 2011.

[11] S. Han, "Modified grey-wolf algorithm optimized fractional-order sliding mode control for unknown manipulators with a fractional-order disturbance observer," *IEEE Access*, vol. 8, pp. 18337–18349, 2020.

[12] X. Zhang and Y. Quan, "Adaptive fractional-order non-singular fast terminal sliding mode control based on fixed time disturbance observer for manipulators," *IEEE Access*, vol. 10, pp. 76504–76511, 2022.

[13] X. Chuanfang, "Finite-time fault-tolerant tracking control of high-speed trains," *J. Railway*, vol. 43, no. 11, pp. 69–77, 2021.

[14] W. Hai, L. Genfeng, and H. Zhongsheng, "High-speed train data-driven model-free adaptive fault-tolerant control," *Control Decis.*, vol. 37, no. 5, pp. 1127–1136, 2022.

[15] L. Wenkai, M. Zehui, J. Bin, and D. Wenwen, "Fault diagnosis of train traction system actuator based on adaptive observer," *J. Shandong Univ. Sci. Technol. Natural Sci. Ed.*, vol. 36, no. 5, pp. 60–64, 2017.

[16] Y. Hao, X. Yuhang, N. Yuan, L. Shi, and J. Bin, "Security decision-making and control of network systems: A review of fault-tolerant game research," *Control Decision-Making*, vol. 37, no. 4, pp. 769–781, 2022.

[17] Z. Mao, X. Yan, B. Jiang, and M. Chen, "Adaptive fault-tolerant sliding-mode control for high-speed trains with actuator faults and uncertainties," *IEEE Trans. Intell. Transp. Syst.*, vol. 21, no. 6, pp. 2449–2460, Jun. 2020.

[18] X. Guo and C. K. Ahn, "Adaptive fault-tolerant pseudo-PID sliding-mode control for high-speed train with integral quadratic constraints and actuator saturation," *IEEE Trans. Intell. Transp. Syst.*, vol. 22, no. 12, pp. 7421–7431, Dec. 2021.

[19] S. Liu, B. Jiang, Z. Mao, and S. X. Ding, "Adaptive backstepping based fault-tolerant control for high-speed trains with actuator faults," *Int. J. Control, Autom. Syst.*, vol. 17, no. 6, pp. 1408–1420, Jun. 2019.

[20] H. Dong, X. Lin, S. Gao, B. Cai, and B. Ning, "Neural networks-based sliding mode fault-tolerant control for high-speed trains with bounded parameters and actuator faults," *IEEE Trans. Veh. Technol.*, vol. 69, no. 2, pp. 1353–1362, Feb. 2020.

[21] Q. Song and Y. Song, "Data-based fault-tolerant control of high-speed trains with traction/braking notch nonlinearities and actuator failures," *IEEE Trans. Neural Netw.*, vol. 22, no. 12, pp. 2250–2261, Dec. 2011.

[22] P. Saxena and A. Kothari, "Optimal pattern synthesis of linear antenna array using grey wolf optimization algorithm," *Int. J. Antennas Propag.*, vol. 2016, pp. 1–11, Apr. 2016.
[23] J. C. Yang and W. Long, "Improved grey wolf optimization algorithm for constrained mechanical design problems," *Appl. Mech. Mater.*, vol. 851, pp. 553–558, Aug. 2016.
[24] N. Sihag, "A novel adaptive grey wolf optimizer for global numerical optimization," *Int. J. Res. Appl. Sci. Eng. Technol.*, vol. 7, no. 11, pp. 524–534, Nov. 2019.
[25] N. Singh and S. B. Singh, "Hybrid algorithm of particle swarm optimization and grey wolf optimizer for improving convergence performance," *J. Appl. Math.*, vol. 2017, pp. 1–15, Nov. 2017.
[26] M. M. Fouad, A. I. Hafez, A. E. Hassanien, and V. Snasel, "Grey wolves optimizer-based localization approach in WSNs," in *Proc. 11th Int. Comput. Eng. Conf. (ICENCO)*, Dec. 2015, pp. 256–260.
[27] S. Zhang, Y. Zhou, Z. Li, and W. Pan, "Grey wolf optimizer for unmanned combat aerial vehicle path planning," *Adv. Eng. Softw.*, vol. 99, pp. 121–136, Sep. 2016.
[28] M. R. Mosavi, M. Khishe, and A. Ghamgosar, "Classification of sonar data set using neural network trained by gray wolf optimization," *Neural Netw. World*, vol. 26, no. 4, pp. 393–415, 2016.
[29] I. Aljarah, M. Mafarja, A. A. Heidari, H. Faris, and S. Mirjalili, "Clustering analysis using a novel locality-informed grey wolf-inspired clustering approach," *Knowl. Inf. Syst.*, vol. 62, no. 2, pp. 507–539, Feb. 2020.
[30] W. Bai, Z. Lin, H. Dong, and B. Ning, "Distributed cooperative cruise control of multiple high-speed trains under a state-dependent information transmission topology," *IEEE Trans. Intell. Transp. Syst.*, vol. 20, no. 7, pp. 2750–2763, Jul. 2019.
[31] L. Zhu, X. Li, D. Huang, H. Dong, and L. Cai, "Distributed cooperative fault-tolerant control of high-speed trains with input saturation and actuator faults," *IEEE Trans. Intell. Vehicles*, vol. 8, no. 2, pp. 1241–1251, Feb. 2023.
[32] S. Jouaber, S. Bonnabel, S. Velasco-Forero, and M. Pilté, "NNAKF: A neural network adapted Kalman filter for target tracking," in *Proc. IEEE Int. Conf. Acoust., Speech Signal Process. (ICASSP)*, Jun. 2021, pp. 4075–4079.
[33] N. Wassiliadis, T. Herrmann, L. Wildfeuer, C. Reiter, and M. Lienkamp, "Comparative study of state-of-charge estimation with recurrent neural networks," in *Proc. IEEE Transp. Electrific. Conf. Expo. (ITEC)*, Jun. 2019, pp. 1–6.
[34] H. Ahmed, S. Biricik, H. Komurcugil, S. B. Elghali, and M. Benbouzid, "Enhanced frequency-adaptive self-tuning filter-based continuous terminal sliding mode control of single-phase dynamic voltage restorer," *Control Eng. Pract.*, vol. 128, Nov. 2022, Art. no. 105340.
[35] M. Gori and M. Maggini, "Optimal convergence of on-line backpropagation," *IEEE Trans. Neural Netw.*, vol. 7, no. 1, pp. 251–254, Jan. 1996.
[36] H. K. Khalil, *Nonlinear Control*. Upper Saddle River, NJ, USA: Prentice-Hall, 2014.
[37] S. Kumari and R. Kumar, "Hybridized GWO-RUN optimized fractional order control for permanent magnet brush-less DC motor,," *Eng. Res. Exp.*, vol. 91, pp. 1720–1731, Mar. 2019.
[38] Z. Qinglong, "Analysis of RAMS characteristics of fuxing multiple unit," *Railway Rolling Stock*, vol. 41, no. 2, pp. 42–46, 2021.
[39] Z. Yu, Y. Zhang, B. Jiang, C.-Y. Su, J. Fu, Y. Jin, and T. Chai, "Fractional order PID-based adaptive fault-tolerant cooperative control of networked unmanned aerial vehicles against actuator faults and wind effects with hardware-in-the-loop experimental validation," *Control Eng. Pract.*, vol. 114, Sep. 2021, Art. no. 104861.
[40] Q. He, X. Mu, and G. Cheng, "Finite time adaptive fault-tolerant controller based on neural networks for switched stochastic nonlinear systems with actuator failures and disturbance," *Int. J. Adapt. Control Signal Process.*, vol. 36, no. 1, pp. 17–37, Jan. 2022.

BINCHUAN LIANG was born in 1997. He received the B.E. degree in transportation equipment and control engineering from Dalian Jiaotong University, in 2021, where he is currently pursuing the master's degree with the College of Automation and Electrical Engineering. His research interests include train network control technology and nonlinear systems.

TONG ZHANG was born in 1977. She received the B.S. degree in physics from Northeastern University, China, in 1999, the M.S. degree in control theory and control engineering from Herbing Engineering University, in 2004, and the Ph.D. degree in control theory and control engineering from the Beijing Institute of Technology, in 2007. She is currently an Associate Professor with Dalian Jiaotong University, Dalian, China. Her research interests include high-speed train network control and intelligent control.